XLI CILAMCE
XLI Ibero-Latin American Congress on Computational Methods in Engineering
16-19 November, 2020 FOZ DO IGUAÇU PARANÁ – BRAZIL

A STABILIZED PRIMAL HYBRID FINITE ELEMENT FORMULATION FOR THE ELASTIC WAVE EQUATION

Juliano D. B. Santos[1],Abimael F. D. Loula[2]

[1]*Laboratório Nacional de Computação Cientıífica*
Av. Getúlio Vargas, 333 – Petrópolis-RJ – CEP: 25.651-075 – Brasil
juliano@lncc.br
[2]*Laboratório Nacional de Computação Cientıfica*
Av. Getúlio Vargas, 333 – Petrópolis-RJ – CEP: 25.651-075 – Brasil
aloc@lncc.br

Abstract. We present a stabilized hybrid finite element formulation for the elastic wave equation in two space dimensions. The proposed hybrid formulation is characterized by the introduction of auxiliary variables on the edges of the elements, which are identified as Lagrange multipliers associated with the trace of displacement field. A second order explicit finite difference method is adopted in the time domain. It is well known that when this second order "explicit" finite difference approximation in time is combined with classical Continuous Galerkin finite element approximations in space it does not lead to a really explicit method, given that the consistent mass matrix in this case is non diagonal. With the proposed formulation it is possible to obtain really explicit methods with block-diagonal mass matrices. Even diagonal mass matrices can also be obtained, as long as the Lagrangian interpolation functions are centered in the Gauss integration points. Convergence studies are conducted on uniform and on randomly generated non-uniform quadrilateral meshes. Meshes with straight or curved quadrilateral elements are considered, associated with Lagrangian bases and with Qk and Pk monomial bases.

Keywords: Elastic Wave, Curved Meshes, Hybrid Method

1 Introduction

This work is dedicated to the proposal of a symmetrical and stabilized primal hybrid formulation for the time elastic wave equation. Mixed finite element hybrid methods have been proposed for solving many important problem in Computational Mechanics and Engineering. In particular, for problems governed by the acoustic and elastic wave equations we refer to the works [1],[2],[3]. One of the advantages of mixed-hibridized methods for elasticity problems is the gain of accuracy in the approximation of stress fields. However, the introduction of additional unknowns, proper of these methods, increases the computational cost for solving the local problems. In [4] is proposed and analyzed a stabilized primal hybrid formulation for the elasticity problem. Later on, hybrid finite element methods are proposed in [5] for the elastic wave equation in the frequency domain in which the multiplier is identified as the trace of the primal variable on the edges of the elements. These last two references are fundamental for the preset work, whose objective is to develop a stabilized primal hybrid formulation for elastic waves in the time domain, with the use of discontinuous function spaces to approximate the multiplier.

2 Notations and definitions

In this section we extend to the primal hybrid formulation proposed and analyzed in [4] for stationary elasticity to the time dependent elasticity problem. Before the introduction of the primal hybrid formulation we present some useful definitions and notations. Let $\mathbb{R}^d$, $d \geq 1$, denote a bounded domain with smooth contour $\partial\Omega$. Given a scalar function space $V(\Omega)$, we introduce the spaces $\boldsymbol{V}(\Omega) = [V(\Omega)]^d$ and $\mathbb{V}(\Omega) = [V(\Omega)]^{d\times d}$ of vector and tensor fields whose components belong to $V(\Omega)$. These spaces are provided with norms, defined in a similar way to the norm of the $V(\Omega)$ space. We defined $\mathcal{T}_h = \{K\}$ the union of all elements K as a regular finite element partition of Ω and denote the set of all edges of the elements by $\mathcal{E}_h = \{e \,:\, e \text{ is an edge of } K \text{ for all } K \in \mathcal{T}_h\}$. The

set of all inner edges, in turn, is denoted by $\mathcal{E}_h^0 = \{e \in \mathcal{E}_h \ : \ e \text{ is an internal edge}\}$ and the set of edges located in the contour of Ω is denoted by $\mathcal{E}_h^\partial = \mathcal{E}_h \cap \Gamma$. To each edge e we associate a normal vector $\boldsymbol{n}_e$.

In the $\mathcal{T}_h$ partition let K^+ and K^- be two any elements containing the same edge e , as illustrated by the Figure (1). On the set of adjacent edges $e = \partial K^+ \cap \partial K^-$, we take an arbitrary point $\boldsymbol{x} \in e$ and exterior unitary normal $\boldsymbol{n}^+$ and $\boldsymbol{n}^-$, respectively, departing from this point. We also need to define jump and average operators for vector $\boldsymbol{v}$ and tensor $\boldsymbol{\tau}$ functions, respectively. functions these smooth inside each element $K^\pm$. Averages in $\boldsymbol{x} \in e$ are defined as $\{\!\{\boldsymbol{v}\}\!\} = \frac{1}{2}(\boldsymbol{v}^+ + \boldsymbol{v}^-)$, $\{\!\{\boldsymbol{\tau}\}\!\} = \frac{1}{2}(\boldsymbol{\tau}^+ + \boldsymbol{\tau}^-)$, in $e \in \mathcal{E}_h^0$, and scalar and vector jumps are denoted in each case by $[\![\boldsymbol{v}]\!] = \boldsymbol{v}^+ \cdot \boldsymbol{n}^+ + \boldsymbol{v}^- \cdot \boldsymbol{n}^-$, $[\![\boldsymbol{\tau}]\!] = \boldsymbol{\tau}^+\boldsymbol{n}^+ + \boldsymbol{\tau}^-\boldsymbol{n}^-$. When $\boldsymbol{x}$ belongs to an edge $e \in \mathcal{E}_h^\partial$, the averages and jumps operators are defined as $\{\!\{\boldsymbol{v}\}\!\} = \boldsymbol{v}$, $\{\!\{\boldsymbol{\tau}\}\!\} = \boldsymbol{\tau}$, and $[\![\boldsymbol{v}]\!] = \boldsymbol{v}\boldsymbol{n}$, $[\![\boldsymbol{\tau}]\!] = \boldsymbol{\tau}\boldsymbol{n}$, with $\boldsymbol{n}$ being the normal unit outside the contour Γ. The jump of a vector to matrix values $[\![\cdot]\!]$ is defined as $[\![\boldsymbol{v}]\!] = \boldsymbol{v}^+ \otimes \boldsymbol{n}^+ + \boldsymbol{v}^- \otimes \boldsymbol{n}^-$, when $\boldsymbol{x} \in \mathcal{E}_h^0$, and $[\![\boldsymbol{v}]\!] = \boldsymbol{v} \otimes \boldsymbol{n}$, if $\boldsymbol{x} \in \mathcal{E}_h^\partial$.

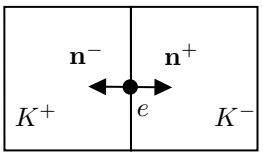

Figure 1. Example of elements with a interface $e = \partial K^+ \cap \partial K^-$.

2.1 Model problem

Let Ω be an open and bounded domain in $\mathbb{R}^2$ with boundary $\partial\Omega = \Gamma$ smooth by parts. We postulate Ω as the domain of an elastic, homogeneous and isotropic body, submitted to an external force $\boldsymbol{f}$. The mathematical model describing elastic wave propagation problem consists in finding the vector field $\boldsymbol{u}(x_1, x_2)$ which satisfies the partial differential equation

$$\begin{cases} \rho\dfrac{\partial^2 \boldsymbol{u}}{\partial t^2} & -\text{div}\boldsymbol{\sigma}(\boldsymbol{u}) = \boldsymbol{f}, \ \text{ in } \Omega, \\ & \boldsymbol{\sigma}(\boldsymbol{u}) = \mathbb{D}\boldsymbol{\varepsilon}(\boldsymbol{u}), \ \text{ in } \ \Omega, \end{cases} \tag{1}$$

subject to boundary condition $\boldsymbol{u} = \boldsymbol{g}$ in Γ and initial conditions $\boldsymbol{u}(\boldsymbol{x}, \boldsymbol{0}) = \boldsymbol{u_0}(\boldsymbol{x})$, $\dfrac{\partial \boldsymbol{u}(\boldsymbol{x}, \boldsymbol{0})}{\partial t} = \boldsymbol{v_0}(\boldsymbol{x})$. Where ρ is the density of the medium, which we will considered here as constant, $\boldsymbol{\sigma}$ is the symmetric Cauchy stress tensor, $\boldsymbol{\varepsilon}(\boldsymbol{u}) = \frac{1}{2}(\nabla\boldsymbol{u} + \nabla\boldsymbol{u}^T)$ is the linear strain tensor, $\mathbb{D} = 2\mu\mathbb{I} + \lambda\boldsymbol{I} \otimes \boldsymbol{I}$ is the isotropic elasticity tensor, where $\boldsymbol{I}$ is the second-order identity tensor and $\mathbb{I}$ is the fourth-order identity tensor on symmetric second-order tensors. For plane strain problems the Lamé coefficients are given by the relations

$$\lambda = \frac{E\upsilon}{(1+\upsilon)(1-2\upsilon)}, \ \ \mu = \frac{E}{2(1+\upsilon)},$$

with E and υ being the modules of elasticity and Poisson coefficient, respectively.

Model(1) is capable of describing pressure and shear wave propagations [6],[7],[8]. Considering a harmonic behavior in time for the displacement field $\boldsymbol{u}$ both a pressure wave $\boldsymbol{u}_p$ and shear waves $\boldsymbol{u}_s$ are solutions to the model problem, separately or combined. One solution, which will be used here in numerical experiments in the following sections, is associated with pressure wave $\boldsymbol{u} = e^{i\omega t}\boldsymbol{u}_p$ where

$$\boldsymbol{u}_p = \alpha_p \begin{pmatrix} \cos\theta \\ \sin\theta \end{pmatrix} e^{ik_p(x_1\cos\theta + x_2\sin\theta)}, \quad k_p = \sqrt{\frac{\lambda + 2\mu}{\rho}},$$

with α_p being the amplitude and k_p the pressure wave number.

2.2 Stabilized primal hybrid method (SPHM)

Initially we introduced the approximation spaces for the displacement field $\boldsymbol{u}$ and for the Lagrange multiplier $\boldsymbol{\lambda} = \mathbf{u}|_{\mathbf{e}}$, which is an auxiliary variable defined on each edge $e \in \mathcal{E}_h$ associate with the trace of the displacement field on each edge e $\mathcal{E}_h^0$. We define the following spaces for the displacement field and the multiplier in this order

$$\boldsymbol{V}_h^k = \{\boldsymbol{v}_h \in \boldsymbol{L}^2(\Omega) : \boldsymbol{v}_h|_K \in [S_k(K)]^2 \ \forall K \in \mathcal{T}_h\} \ \text{ and } \quad \boldsymbol{M}_h^l = \{\boldsymbol{\lambda} \in \boldsymbol{L}^2(\mathcal{E}_h) : \boldsymbol{\lambda}|_e = [p_l(e)]^2, \forall e \in \mathcal{E}_h^0\}.$$

For the displacement approximation we adopt $S_k(K) \in \{\mathbb{Q}_k(K), \mathbb{P}_k(K)\}$ and for the multiplier we consider $p_l(e)$, space of discontinuous polynomials of degree $\leq l$ in each edge e. By construction, functions $\boldsymbol{v}_h$ belonging to broken function space $\boldsymbol{V}_h^k$ are defined, independently, in each element K belonging to the partition. Our primal hybrid formulation will be applied to meshes of quadrilateral elements, without loss of generality. In fact, the hybrid method can be performed on generic polygonal partitions. Restricted to an element K the model problem (1) can be rewritten as:

Finding a displacement field $\boldsymbol{u}$ satisfying the equation

$$\rho \frac{\partial^2 \boldsymbol{u}}{\partial t^2} - \operatorname{div}\left(\llbracket \mathbb{D}\boldsymbol{\varepsilon}(\boldsymbol{u}) \rrbracket\right) = \boldsymbol{f}, \ \text{ in } K, \tag{2}$$

and the interface conditions

$$\llbracket \mathbb{D}\boldsymbol{\varepsilon}(\boldsymbol{u}) \rrbracket_e = \boldsymbol{0}, \quad [\![\boldsymbol{u}]\!]_e = \boldsymbol{0}, \tag{3}$$

on each edge $e \in \mathcal{E}_h^0$. The semi-discreet stabilized primal hybrid formulation on each element K, for the problem (2) consists, for $\rho = 1$, in :

Finding the pair $[\boldsymbol{u}_h, \boldsymbol{\lambda}_h] \in \boldsymbol{V}_h^k \times \boldsymbol{M}_h^l$ such that, for all $[\boldsymbol{v}_h, \boldsymbol{\mu}_h] \in \boldsymbol{V}_h^k \times \boldsymbol{M}_h^l$

$$\begin{aligned}
&\sum_{K\in\mathcal{T}_h} \int_K \frac{\partial^2 \boldsymbol{u}_h}{\partial t^2} \cdot \boldsymbol{v}_h dx + \sum_{K\in\mathcal{T}_h} \int_K \mathbb{D}\boldsymbol{\varepsilon}(\boldsymbol{u_h}) : \boldsymbol{\varepsilon}(\boldsymbol{v_h}) dx - \sum_{K\in\mathcal{T}_h} \int_{\partial K} \mathbb{D}\boldsymbol{\varepsilon}(\boldsymbol{u_h})\boldsymbol{n}_k \cdot (\boldsymbol{v}_h - \boldsymbol{\mu}_h) ds \\
&- \sum_{K\in\mathcal{T}_h} \int_{\partial K} \mathbb{D}\boldsymbol{\varepsilon}(\boldsymbol{v_h})\boldsymbol{n}_k \cdot (\boldsymbol{u}_h - \boldsymbol{\lambda}_h) ds + 2\mu \sum_{K\in\mathcal{T}_h} \beta_1 \int_{\partial K} (\boldsymbol{u}_h - \boldsymbol{\lambda}_h) \cdot (\boldsymbol{v}_h - \boldsymbol{\mu}_h) ds = \sum_{K\in\mathcal{T}_h} \int_K \boldsymbol{f} \cdot \boldsymbol{v}_h dx,
\end{aligned} \tag{4}$$

where $\beta_1 = \frac{\beta_0}{h}$, $\beta_0 \geq 0$. Applying some identities given in [4] the integral equation (4), for $\boldsymbol{\lambda}_h$ and $\boldsymbol{\mu}_h$ only determined, can be rewritten as:

Find the pair $[\boldsymbol{u}_h, \boldsymbol{\lambda}_h] \in \boldsymbol{V}_h^k \times \boldsymbol{M}_h^l$ such that

$$A([\boldsymbol{u}_h, \boldsymbol{\lambda}_h], [\boldsymbol{v}_h, \boldsymbol{\mu}_h]) = \boldsymbol{F}([\boldsymbol{v}_h, \boldsymbol{\mu}_h]), \ \forall [\boldsymbol{v}_h, \boldsymbol{m}_h] \in \boldsymbol{V}_h^k \times \boldsymbol{M}_h^l,$$

with

$$\begin{aligned}
A([\boldsymbol{u}_h, \boldsymbol{\lambda}_h], [\boldsymbol{v}_h, \boldsymbol{\mu}_h]) &= a_{DG}(\boldsymbol{u}_h, \boldsymbol{v}_h) - \sum_{e\in\mathcal{E}_h^0} \int_e \llbracket \mathbb{D}\boldsymbol{\varepsilon}(\boldsymbol{v_h}) \rrbracket \cdot (\{\!\{\boldsymbol{u}_h\}\!\} - \boldsymbol{\lambda}_h) ds \\
&\sum_{e\in\mathcal{E}_h^0} \int_e -\llbracket \mathbb{D}\boldsymbol{\varepsilon}(\boldsymbol{u_h}) \rrbracket \cdot (\{\!\{\boldsymbol{v}_h\}\!\} - \boldsymbol{\mu}_h) ds + 2\mu \sum_{K\in\mathcal{T}_h} \frac{\beta_0}{2h} \int_{\partial K} (\boldsymbol{u}_h - \boldsymbol{\lambda}_h) \cdot (\boldsymbol{v}_h - \boldsymbol{\mu}_h) ds, \\
\boldsymbol{F}([\boldsymbol{v}_h, \boldsymbol{\mu}_h]) &= \sum_{K\in\mathcal{T}_h} \int_K \boldsymbol{f} \cdot \boldsymbol{v}_h dx,
\end{aligned} \tag{5}$$

in which

$$\begin{aligned}
a_{DG}(\boldsymbol{u}_h, \boldsymbol{v}_h) = &\sum_{K\in\mathcal{T}_h} \int_K \frac{\partial^2 \boldsymbol{u}_h}{\partial t^2} \cdot \boldsymbol{v}_h dx + \sum_{K\in\mathcal{T}_h} \int_{\partial K} \mathbb{D}\boldsymbol{\varepsilon}(\boldsymbol{u_h}) : \boldsymbol{\varepsilon}(\boldsymbol{v_h}) dx - \sum_{e\in\mathcal{E}_h} \int_e \{\!\{\mathbb{D}\boldsymbol{\varepsilon}(\boldsymbol{u_h})\}\!\} : \llbracket \boldsymbol{v}_h \rrbracket ds \\
&- \sum_{e\in\mathcal{E}_h} \int_e \{\!\{\mathbb{D}\boldsymbol{\varepsilon}(\boldsymbol{v_h})\}\!\} : \llbracket \boldsymbol{u}_h \rrbracket ds + 2\mu \sum_{e\in\mathcal{E}_h} \frac{\beta_0}{2h} \int_e \llbracket \boldsymbol{u}_h \rrbracket : \llbracket \boldsymbol{v}_h \rrbracket ds.
\end{aligned} \tag{6}$$

As observed in [4], by solving exactly the multiplier equation we have

$$\boldsymbol{\lambda}_h = \{\boldsymbol{u}_h\} - \frac{1}{2\beta_0 2\mu} \llbracket \mathbb{D}\boldsymbol{\varepsilon}(\boldsymbol{u_h}) \rrbracket, \tag{7}$$

and replacing (7) in the hybrid formulation (5), we obtained the following modified Discontinuous Galerkin method

$$A([\boldsymbol{u}_h, \boldsymbol{\lambda}_h], [\boldsymbol{v}_h, \boldsymbol{\mu}_h]) = a_{DG}(\boldsymbol{u}_h, \boldsymbol{v}_h) - \frac{1}{2\mu} \sum_{e\in\mathcal{E}_h} \int_e \frac{1}{2\beta_0} \llbracket \mathbb{D}\boldsymbol{\varepsilon}(\boldsymbol{u_h}) \rrbracket \cdot \llbracket \mathbb{D}\boldsymbol{\varepsilon}(\boldsymbol{v_h}) \rrbracket ds, \tag{8}$$

where the latter term is the only difference of this modified method to the classic Symmetric Interior Penalty Discontinuous Galerkin formulation.

3 Time integration algorithm

For a totally discrete version of the equation(4), the mid-point rule will be applied in the approximation of the temporal derivative. This way an explicit method will be obtained, having as initial conditions the displacement fields in $t = 0$ and $t = \Delta t$. Being Δt the integration step in time and h the mesh refinement parameter, we formulate the following explicit algorithm:

Given $\boldsymbol{u}_h^0 = \boldsymbol{u}_h(x_1, x_2, 0)$, $\boldsymbol{u}_h^1 = \boldsymbol{u}_h(x_1, x_2, \boldsymbol{\Delta t})$ *find* $[\boldsymbol{u}_h^{n+1}, \boldsymbol{\lambda}_h^n] \in \boldsymbol{V}_h^k \times \boldsymbol{M}_h^l$ *such that*

$$\boldsymbol{\lambda}_h^n = \{\boldsymbol{u}_h^n\} - \frac{1}{2\beta_0 2\mu}[\![\mathbb{D}\boldsymbol{\varepsilon}(\boldsymbol{u_h^n})]\!], \quad \textit{for every edge } e \in \varepsilon_h^0 \tag{9}$$

$$\int_K \frac{\boldsymbol{u}_h^{n+1} - 2\boldsymbol{u}_h^n + \boldsymbol{u}_h^{n-1}}{\Delta t^2} \cdot \boldsymbol{v}_h dx + \int_K \mathbb{D}\boldsymbol{\varepsilon}(\boldsymbol{u_h^n}) : \boldsymbol{\varepsilon}(\boldsymbol{v_h}) dx - \int_{\partial K} \mathbb{D}\boldsymbol{\varepsilon}(\boldsymbol{u_h^n})\boldsymbol{n}_k \cdot \boldsymbol{v}_h ds$$
$$- \int_{\partial K} \mathbb{D}\boldsymbol{\varepsilon}(\boldsymbol{v_h})\boldsymbol{n}_k \cdot (\boldsymbol{u}_h^n - \boldsymbol{\lambda}_h^n) ds + 2\mu\beta_0 \int_{\partial K} (\boldsymbol{u}_h^n - \boldsymbol{\lambda}_h^n) \cdot \boldsymbol{v}_h ds = \int_K \boldsymbol{f} \cdot \boldsymbol{v}_h dx, \ \forall \boldsymbol{v}_h \in \boldsymbol{V}_h^k, \tag{10}$$

for each element $K \in \mathcal{T}_h$. In matrix form, the equation (10) is presented in each element as

$$\boldsymbol{M}(\boldsymbol{U}^{n+1} - 2\boldsymbol{U}^n + \boldsymbol{U}^{n-1}) + \boldsymbol{K}\boldsymbol{U}^n = \boldsymbol{F}^n \tag{11}$$

$$\Rightarrow \boldsymbol{U}^{n+1} = 2\boldsymbol{U}^n - \boldsymbol{U}^{n-1} + \boldsymbol{M}^{-1}(\boldsymbol{F}^n - \boldsymbol{K}\boldsymbol{U}^n), \tag{12}$$

where $\boldsymbol{M}$ is the mass matrix, $\boldsymbol{K}$ is the stiffness matrix that incides on volume integrals and edge integrals on $\boldsymbol{u}_h^n$ and $\boldsymbol{F}^n$ is the vector that incides on edge integrals on $\boldsymbol{\lambda}_h^n$ and source term. When adopting Lagrangian polynomials as basis functions for $\boldsymbol{V}_h^k$ we consider two situations: (1) Lagrange polynomials centered in the nodal points and (2) Lagrange polynomials centered in the Gauss integration points. In the first case, the mass matrix will be block-diagonal. In the second case, the mass matrix will be diagonal. When monomial in $\mathbb{P}_2$ or $\mathbb{Q}_2$ are adopted as basis functions, the associated mass matrices will always be block-diagonal.

4 Convergence studies

Numerical experiments will be carried out on meshes of uniform and randomly deformed quadrilateral elements to test the convergence rates of the proposed stabilized hybrid method when adopting $\mathbb{Q}_2$ Lagrangian bases and $\mathbb{Q}_2$ and $\mathbb{P}_2$ monomial bases in the physical variables x and y [9], with no mapping. The L^2-projections of initial conditions and the exact solution are calculated to be compared with the approximations provided by the proposed hybrid method. This projection, denoted by $\tilde{u}_h$, is given by

$$(\tilde{u}_h, v_h)_K = (u, v_h)_K, \ \forall v_h \in V_h,$$

in each element $K \in \mathcal{T}_h$. Approximations will be made on meshes of $2^{i+1} \times 2^{i+1}$ elements and respective $n_{stp} = 80 \times 2^{i+1}$ time steps , with $i = 0, 1, 2, 3, 4$, using polynomials $\mathbb{Q}_2$ and $\mathbb{P}_2$. The non-uniform meshes will be generated by random perturbations in the (x_j, y_j) coordinates of the nodes inside the domain. This is done by redefining coordinates $x_j^* := x_j + \delta \cdot \ rand \cdot h$, $y_j^* := y_j + \delta \cdot \ rand \cdot h$ being $\delta := 0,14$ the perturbation percentage, $rand$ a pseudo random number in the range $[-1, 1]$ and h the original length on the side of the element in the uniform mesh. As a exact solution the real part of the field will be adopted $\boldsymbol{u} = e^{i\omega t}\boldsymbol{u}_p$ where $\boldsymbol{u}_p = \alpha_p \begin{pmatrix}\cos\theta & \sin\theta\end{pmatrix}^T e^{ik_p(x\cos\theta + y\sin\theta)}$, with amplitude $\alpha_p = 1$. The problem parameters (1) will be constants with values $\omega = 4$, $\rho = 1$, $\theta = \pi/4$ and Lamé parameters fixed at $E = 1$ and $\upsilon = 0,3$. The approximate solutions were obtained using quadrilateral elements $\mathbb{P}_k - p_k$ and $\mathbb{Q}_k - p_k$, where k denotes the degree of polynomial space for the displacement field and the Lagrange multiplier. All results of the convergence studies correspond to the final instant $t = Tf = 1(s)$.

In Figure 2 are presented the graphs that confront the approximations via DG and SPHM in sequences of uniform and deformed meshes of $\mathbb{Q}_2$ elements and Lagrangian function spaces. The expected rates are observed on uniform meshes for the approximations of the displacements in the L^2-norm for both methodologies in the first three meshes. The SPHM approximations are more accurate. With h refiniement, it is observed that the error of second order temporal discretization begins to predominate in the last meshes of the sequence (Figure 2(a)). The gradient approximations in both methods present optimal rates in the whole sequence of uniform meshes (Figure 2(b)), for being second order in bothe space and time approximations. The Figures 2(c) e 2(d) present the results

associated with the approximations of the displacements and their gradients over sequences of deformed meshes. In this case, the elements will not have straight sides and a geometric transformation is necessary to define elements with curved sides [10], causing sub-optimal rates of convergence for the displacements and their gradients. In this scenario the SPHM method presents a gain of accuracy in the whole sequence of meshes for the displacement and also for the stress.

Experiments with monomial function spaces $\mathbb{Q}_2 - p_2$ with both methods can be seen in Figures 3. For uniform meshes a behavior analogous to that of SPHM with Lagrangian basis functions is observed. For non-uniform meshes, the rates of convergence of the approximations obtained by both methods deteriorate. This is due to the fact that the traces of the monomials belonging to $\mathbb{Q}_2$ do not always belong to $p_2(e)$, when the edge e is not aligned with the x or y coordinated axis.

Other h-convergence study is presented in Figure 4 with approximations via DG and SPHM in sequences of uniform and deformed meshes and $\mathbb{P}_2 - p_2$ monomial function spaces. In this case, we can clearly observe that the convergence behavior of both DG and SPHM is not affected by the mesh distortion. The expected rates of convergence are observed for the displacements (Figures 4(a) and 4(c)), gradient of displacement(Figures 4(b) and 4(d).

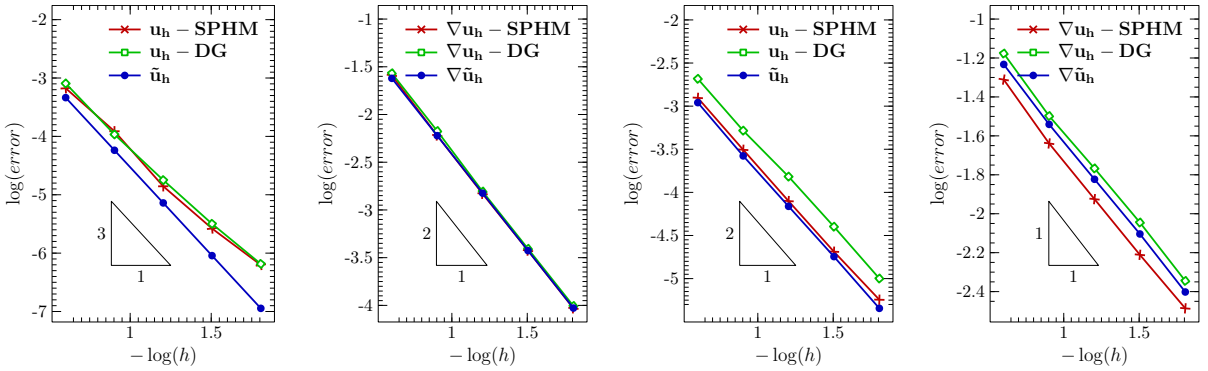

(a) L^2-norm in uniform mesh sequence.

(b) H^1 semi-norm in sequence of uniform meshes.

(c) L^2-norm in sequence of deformed meshes.

(d) H^1 semi-norm in sequence of deformed meshes.

Figure 2. Convergence study in the L^2-norm and H^1 semi-norm of the approximations $\mathbf{u}_h$ obtained with the DG and SPHM methods, compared with the projection $\tilde{\mathbf{u}}_h$, for Lagrangian function spaces $\mathbb{Q}_2$ with nine node elements, considering uniform meshes (Figures (a) and (b)) and randomly distorted meshes (Figures (c) and (d)).

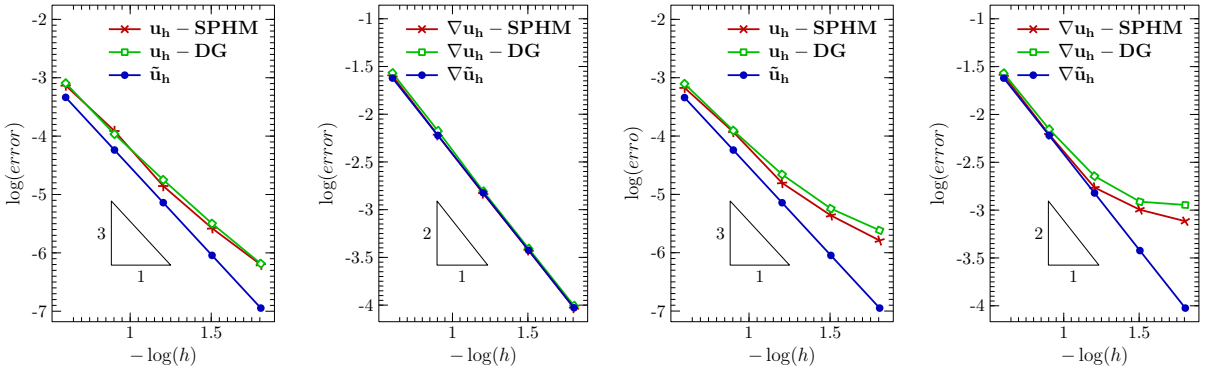

(a) L^2-norm in uniform mesh sequence.

(b) H^1 semi-norm in sequence of uniform meshes.

(c) L^2-norm in sequence of deformed meshes.

(d) H^1 semi-norm in sequence of deformed meshes.

Figure 3. Convergence study in the L^2-norm and H^1 semi-norm of the approximations $\mathbf{u}_h$ obtained with DG and SPHM, compared with the projection $\tilde{\mathbf{u}}_h$, for spaces of monomial $\mathbb{Q}_2$ with nine node elements, considering uniform meshes (Figures (a) and (b)) and randomly distorted meshes (Figures (c) and (d)).

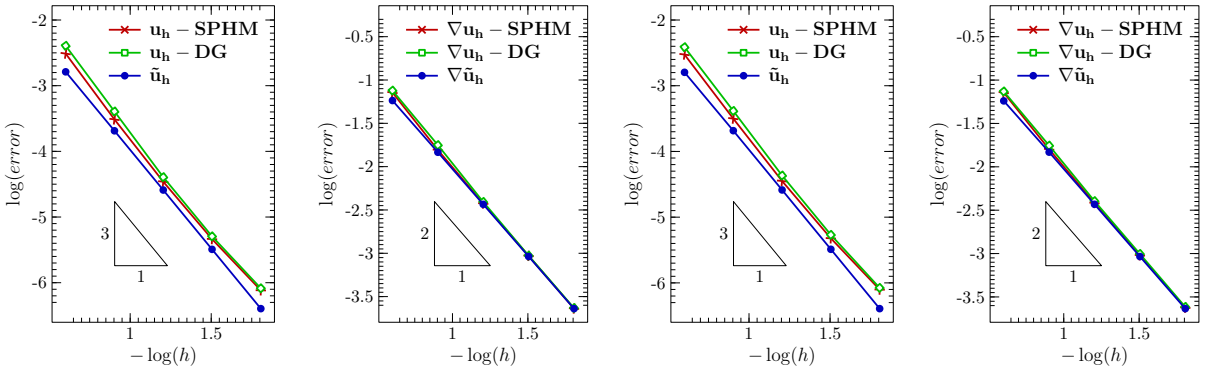

(a) L^2-norm in uniform mesh sequence. (b) H^1 semi-norm in sequence of uniform meshes. (c) L^2-norm in sequence of deformed meshes. (d) H^1 semi-norm in sequence of deformed meshes.

Figure 4. Convergence study in the L^2-norm and H^1 semi-norm of the approximations $\mathbf{u}_h$ obtained with DG and SPHM, compared with the projection $\tilde{\mathbf{u}}_h$, for spaces of monomials $\mathbb{P}_2$ on nine node elements, considering uniform meshes (Figures (a) and (b)) and randomly distorted meshes (Figures (c) and (d)).

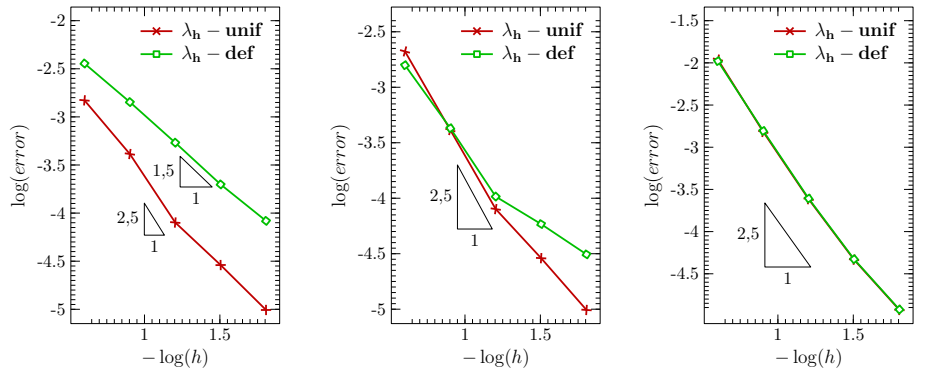

(a) Lagrangian basis and $\mathbb{Q}_2 - p_2$ (b) Monomial basis and $\mathbb{Q}_2 - p_2$ (c) Monomial basis and $\mathbb{P}_2 - p_2$

Figure 5. Convergence study in the L^2-norm for the $\boldsymbol{\lambda}_h$ SPHM approximations with $\beta_0 = 24$ considering different function spaces with quadrilateral elements of 9 nodes $\mathbb{Q}_2$ in randomly distorted meshes.

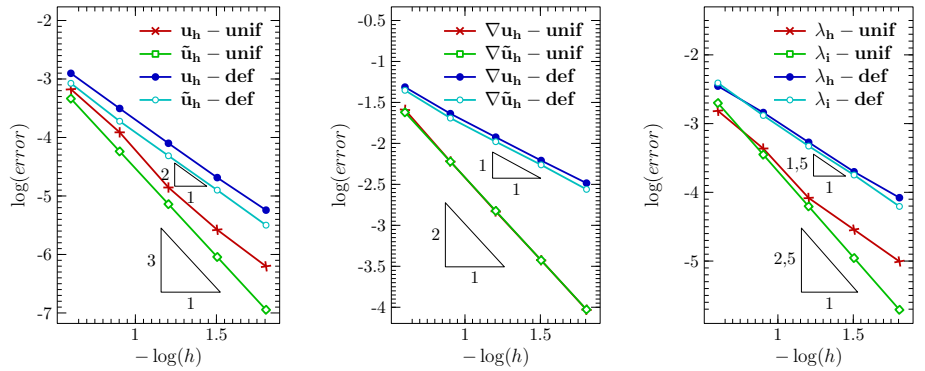

(a) $\boldsymbol{u}_h$ and $\boldsymbol{u}_h$ (b) $\nabla\boldsymbol{u}_h$ and $\nabla\boldsymbol{u}_h$ (c) $\boldsymbol{\lambda}_h$ and $\boldsymbol{\lambda}_i$

Figure 6. SPHM L^2-norm convergence for displacement, gradient of gradient and multiplier, with Lagrangian function spaces $\mathbb{Q}_2 - p_2$ centered in Gauss points considering uniform and randomly deformed meshes.

In [11] a special situation is presented for a formulation of Discontinuous Galerkin in which the obtaining of diagonal mass matrices associated with the temporal discretization of the acoustic wave equation is feasible by using the Lagrangian polynomial base centered on Gauss points. We also adopt Lagrangian bases centered on Gauss integration points in the SPHM formulation for the elastic wave. The corresponding results of convergence studies are presented in Figure 6. For uniform meshes it is possible to observe optimal rates for the L^2-projections

of displacements and their gradients. The influence of the temporal discretization error can also be observed in more refined meshes of the sequence, either in the approximation of the displacement (Figure 6(a)) or the multiplier (Figure 6(c)). Still in uniform meshes, optimal rates are obtained for the approximation of the gradient $\nabla \boldsymbol{u}_h$. Concerning distorted mesh, suboptimal rates of convergence are observed, as expected in the context of Lagrangian approximations functions, as a consequence of the need for the aforementioned mapping.

5 Conclusions

A hybrid stabilized formulation denoted by SPHM is proposed and applied to the elastic wave equation with Dirichlet boundary conditions. The Lagrange multiplier, identified as the trace of the solution in the structure of the mesh composed by the edges of the elements, is calculated from the initial conditions of the problem. As the continuity of the DG and SPHM methods is imposed by the variational, the use of discontinuous monomial function spaces is possible. The $\mathbb{P}_k$ spaces is proved to be more robust on distorted quadrilateral meshes than the $\mathbb{Q}_k$ spaces whose convergence rates are severely affected by mesh distortion.

Acknowledgements The authors thank CAPES, Coordenação de Aperfeiçoamento de Pessoal de Nível Superior, for the financial support to the development of this work.

Authorship statement. The authors hereby confirm that they are the sole liable persons responsible for the authorship of this work, and that all material that has been herein included as part of the present paper is either the property (and authorship) of the authors, or has the permission of the owners to be included here.

References

[1] Nguyen, N. C., Peraire, J., & Cockburn, B., 2011. High-order implicit hybridizable discontinuous galerkin methods for acoustics and elastodynamics. *Journal of Computational Physics*, vol. 230, n. 10, pp. 3695–3718.
[2] Cockburn, B. & Quenneville-Bélair, V., 2014. Uniform-in-time superconvergence of the hdg methods for the acoustic wave equation. *Mathematics of Computation*, vol. 83, n. 285, pp. 65–85.
[3] Fernandez, P., Christophe, A., Terrana, S., Nguyen, N. C., & Peraire, J., 2018. Hybridized discontinuous galerkin methods for wave propagation. *Journal of Scientific Computing*, vol. 77, n. 3, pp. 1566–1604.
[4] Faria, C. O., Loula, A. F., & dos Santos, A. J., 2014. Primal stabilized hybrid and dg finite element methods for the linear elasticity problem. *Computers & Mathematics with Applications*, vol. 68, n. 4, pp. 486–507.
[5] Amad, A. A., Loula, A. F., & Novotny, A. A., 2017. A new method for topology design of electromagnetic antennas in hyperthermia therapy. *Applied Mathematical Modelling*, vol. 42, pp. 209–222.
[6] Rawlinson, N., 1999. Australian National University research school of earth sciences.
[7] Amad, A. A. S., 2016. *Numerical Methods for Time-Harmonic Wave Problems*. PhD thesis, LNCC, Petrópolis.
[8] Wang, S., 2017. *Finite Difference and Discontinuous Galerkin Methods for Wave Equations*. PhD thesis, Acta Universitatis Upsaliensis.
[9] Ainsworth, M. & Oden, J. T., 2011. *A posteriori error estimation in finite element analysis*, volume 37. John Wiley & Sons.
[10] Hughes, T. J. R., 2000. *The Finite Element Method: Linear Static and Dynamic Finite Element Analysis*. Dover Civil and Mechanical Engineering. Dover Publications.
[11] Grote, M. J., Schneebeli, A., & Schötzau, D., 2006. Discontinuous galerkin finite element method for the wave equation. *SIAM Journal on Numerical Analysis*, vol. 44, n. 6, pp. 2408–2431.